Agent-based Models of Cell Aggregation

Thomas M. Brown

April 20, 2013

Abstract

Cell aggregation is a phenomenon common to a wide variety of biological scenarios, one of which is the formation of cell aggregates in liver tissue engineering. Hepatocytes are the most numerous and important cells in the liver, and aggregate *in vitro* to form liver tissue. Experimentally, liver tissue culturing is moving away from mono-layer techniques in favour of three-dimensional environments. The latter facilitate growth of spheroid aggregates, which are emerging as more promising in their structural similarity to organic livers as well as their ability to retain functionality and viability. However, this shift is not reflected in the mathematical literature, in which only two-dimensional models of cell aggregation available. Agent-based modelling is increasingly becoming the method of choice when applied to cellular mechanisms such as aggregation. Agent-based models, discrete both in time and space, consist of a set of rules that dictate each cell's state given its previous state and that of neighbouring cells. Such a model is developed with the aim of mimicking the spatial development and pattern formation observed during the biological process of hepatocyte aggregation *in vitro*. A model of planar aggregation is successfully implemented, and the first stages of three-dimensional aggregate formation are modelled. We show how analysis of the spatial structure (using statistical measures) of both the experimental and simulation domains could be used to to select the agent-based rules that best mimic the cell biology, and hence allow us to gain more insight into the nature of the biological interactions taking place.

Contents

1 Introduction

The liver is one of the largest and most complex organs in humans, with over 500 different functions. The potential for growing functional liver tissue *in vitro* for use in drug testing, or in the longer term, use in liver-assistance devices or for transplant, is a very active area of experimental research. Hepatocytes are liver cells that comprise approximately 80% of a functional liver, and perform the majority of its biological functions (Green et al. 2010). As such, culturing hepatocytes is an important initial step in the growth of liver tissue.

In order to implement the aforementioned applications, the cells in the culture must remain alive (viable) and functional (differentiated) for extended periods. Given certain conditions and culturing techniques, hepatocytes can aggregate to form liver tissue (see Figure 1), and these aggregated structures appear to enhance the functionality and viability of the tissue compared with isolated hepatocytes (Green et al. 2010). Thus, investigating how to promote such aggregation is in the interest of furthering this experimental research.

Historically, hepatocytes have been cultured using mono-layer techniques, producing planar aggregates. More recently, three-dimensional culturing techniques have been employed, producing spherical aggregates, or spheroids. These spheroids are thought to better reflect the architecture of an organic liver, mimicking certain structures particularly well (Abu-Absi et al. (2004)). Whilst there is some detailed knowledge of the mechanisms by which hepatocyte cells form liver tissue, these are many aspects that have not been formalised. The goal of this paper is to seek a better understanding of the hepatocyte aggregation process using agent-based modelling.

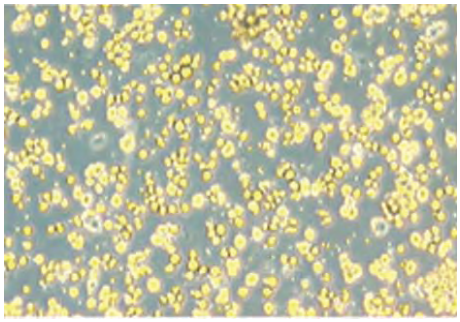

(a) Initial State - 0 Hours

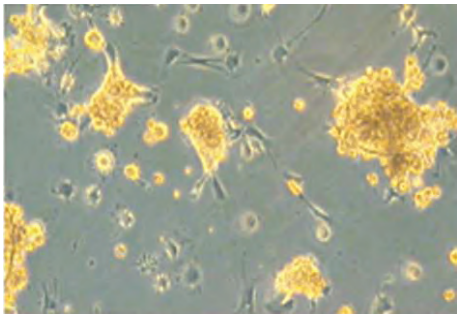

(b) Later State - 48 Hours

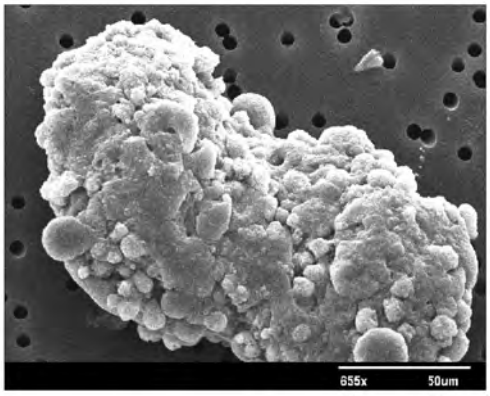

(c) Multicellular liver spheroid

Figure 1: (a) and (b): Images from a time lapse movie provided by Tissue Engineering Group, School of Pharmacy, The University of Nottingham (RJ. Thomas et al. (2006)). The images show hepatocyte cells co-cultured with stellate cells (another type of cell in the liver) forming spheroids. Hepatocyte cells are shown in yellow, stellates in light grey. (c) Scanning electron micrograph of a multicellular liver spheroid (courtesy of L. Riccalton-Banks, Tissue Engineering Group, University of Nottingham)

Morphogenesis describes the development of shape, pattern, or form in an organism. The processes that underlie morphogenesis are rather complex, influenced by factors including genetic determination, environmental influences and interactions with other organisms, cells or chemicals (Edelstein-Keshet (2005)). We ignore many of these processes in order to explore the assumption that aggregation is primarily the result of cell-cell interactions between hepatocytes. Specifically, we seek to develop a model that, given an initial distribution of cells similar to that constructed *in vitro*, produces spatial patterns similar to those observed experimentally.

Agent-based models are often employed to simulate cellular mechanisms, as they reflect the stochastic variability observed in experiments. They also enable analysis of the cell-level and population level behaviour (Binder et al. (2006)), providing a simple and effective way to formalise proposed theories of how a mechanism operates in computational terms. In these models, space is represented as a uniform grid, time advances in discrete steps, and the movement of an agent is dictated by a set of rules based on its previous location and that of neighbouring agents. Compared to other methods, agent-based models are fast and simple to implement, and provide instantaneous visual feedback that allow easy qualitative comparison with experimental images (Ermentrout & Edelstein-Keshet (1993)). This analysis can be extended quantitatively by collecting simulation data from the model using image analysis.

Two agent-based models were developed and implemented: one reflecting planar aggregation, and the other reflecting the early stages of spheroid formation. Given that cellular movement is often a combination of random motion and movement based on interaction with other cells, we develop an agent-based aggregation rule encompassing both deterministic and random components. Our model was able to produce a wide variety of aggregate patterns. The spatial patterns of aggregates produced by the model were then analysed statistically and compared with experimental images.

2 Agent-based Model Formulation

We now develop agent-based models to replicate the aggregation process of a closed population of a single species of cells (hepatocytes) *in vitro*. Unlike biological processes such as the slime mould *dictyostelium discoideum* (Edelstein-Keshet (2005)), in which a single large aggregate is formed, we wish to be able to represent patterns with varying aggregate size and number as seen in experimental images of spheroid aggregate formation (see Figure 1). The most successful model developed, incorporated a combination of deterministic movement based on the location of neighbouring agents, coupled with some random movement. The deterministic component of our model was based on the assumption that aggregation occurs due to cell-cell attraction. Specifically, a given hepatocyte cell scans its local environment for other cells and moves in the direction of highest cell density.

The agent-based models are simulated on a square two-dimensional lattice, with a fixed

constant domain of width X in the x-direction and height Y in the y-direction. The domain consists of sites within the lattice (X, Y), whose positions are located at the discrete integer points (x, y), for $1 \leq x \leq X$ and $1 \leq y \leq Y$. Each of the sites is vacant or occupied by a single square cellular agent. The initial lattice, at time t=0, is populated randomly with a predetermined number cellular agents (fixed population size) N, which remains constant throughout the simulation. This gives rise to a constant domain cell-density $\rho = \frac{N}{XY}$. For simplicity, proliferation and death of cells are neglected, with only motility possible. The assumption that cell proliferation does not occur is realistic as proliferation is limited in experimental contexts where growth factors are not used (Riccalton-Banks et al. (2003)). In addition, cells must remain within the specified domain, ensuring that the population is closed. During a single time step t to $t + 1$, the N cellular agents are selected independently at random, one at a time, and given the opportunity to move. This is called the sequential update method (Simpson et al. (2006)). The stochasticity of this, coupled with that of the random population of the initial system, is thought to reflect the randomness and non-uniformity of the biological process realistically. When a single cellular agent at (x, y) is selected, it moves according to an aggregation rule. According this rule, a given cell will *attempt* to migrate to a lattice site directly above, $(x, y + 1)$, below, $(x, y - 1)$, to the right, $(x + 1, y)$, or the left, $(x - 1, y)$ (see Figure 2). If the site is vacant the move is *successful*,

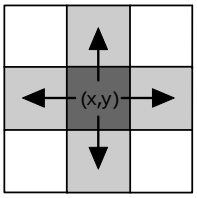

Figure 2: Cell Motility: Possible moves

and the new site becomes occupied by the cell, leaving its previous site empty. If the new site is already occupied by another cell, the move is *aborted*, with the cell retaining its initial position. A cell may only move one lattice site at a time (or not at all), and may not exit the domain.

2.1 Deterministic Component

The deterministic component consists of a majority rule based on density of neighbouring agents, where a given cellular agent moves in the direction of highest density relative to that agent. The density of neighbours is determined by searching in a number of 1D lines of lattice sites called *shells* (see Figure 3). Given a cellular agent at (x, y), consider a collection of L shells extending in the 4 primary directions; y^+, y^-, x^+, x^-. That is, each direction has one, or more, shells associated with it. We call L the *search radius* of a cell. We want to find the

number of agents in each primary direction, given a specified search radius, and move in the direction of highest count.

Given that an empty site is represented as a zero and a site occupied by a cellular agent represented by 1 unit, we can define the indicator function representing occupancy:

$$M(x,y) = \begin{cases} 0 & \text{if site } (x,y) \text{ vacant,} \\ 1 & \text{if site } (x,y) \text{ occupied by cellular agent.} \end{cases}$$

If $L = 1$, we have only the first shell to consider. The first shell in the positive y direction is comprised of lattice sites; $(x-1, y+1), (x, y+1)$ and $(x+1, y+1)$. The first shells in the y^-, x^+ and x^- directions are defined similarly, as shown in Figure 3.

For each primary direction, we consider searching for agents in each of the lattice sites comprising the L shells, and sum the contributions of agent density to obtain a directional count. This will indicate which direction to move in.

Thus for $L = 1$, we obtain the counts:

$$\begin{aligned} y^+_{count} &= M(x-1,y+1) + M(x,y+1) + M(x+1,y+1), \\ y^-_{count} &= M(x-1,y-1) + M(x,y-1) + M(x+1,y-1), \\ x^+_{count} &= M(x+1,y-1) + M(x+1,y) + M(x+1,y+1), \\ x^-_{count} &= M(x-1,y-1) + M(x-1,y) + M(x-1,y+1). \end{aligned}$$

For L larger than 1, we consider the lth shell, for $1 \leq l \leq L$.

The endpoints of the lth shell comprise two of the four diagonals off $(x,y); (x+1, y+l), (x+1, y-l), (x-1, y+l), (x-1, y-l)$, as well as the lattice sites between these endpoints. The lth shell will comprise $2l+1$ lattice sites.

For example, for $L = 2$, the 1^{st} (l=1) and 2^{nd} (l=2) shells are searched (see Figure 3).

For L=2 the following counts are obtained:

$$\begin{aligned} y^+_{count} &= \sum_{i=x-1}^{x+1} M(i,y+1) + \sum_{i=x-2}^{i=x+2} M(i,y+2), \\ y^-_{count} &= \sum_{i=x-1}^{x+1} M(i,y-1) + \sum_{i=x-2}^{i=x+2} M(i,y-2), \\ x^+_{count} &= \sum_{j=y-1}^{y+1} M(x+1,j) + \sum_{j=y-2}^{j=y+2} M(x+2,j), \\ x^-_{count} &= \sum_{j=y-1}^{y+1} M(x-1,j) + \sum_{j=y-2}^{j=y+2} M(x-2,j). \end{aligned}$$

Postal Address: 111 Barry Street
c/- The University of Melbourne
Victoria 3010 Australia

Email: enquiries@amsi.org.au
Phone: +61 3 8344 1777
Fax: +61 3 9349 4106
Web: www.amsi.org.au

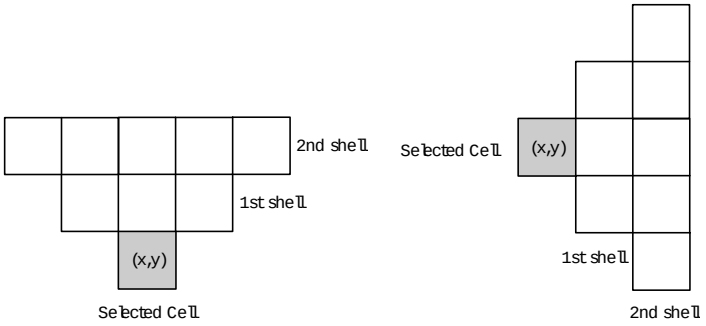

(a) Search area for y^+_{count} (b) Search area for x^+_{count}

(c) Search area for y^-_{count} (d) Search area for x^-_{count}

Figure 3: The search areas for the 4 primary directions, using the shell aggregation rule with $L = 2$. Selected agent at (x, y) represented in grey, the white lattice sites are included in the search.

An example of the cell movement calculation is given in Figure 4.
More generally, for an arbitrary search radius L, the following definitions are relevant:

$$\text{Positive } y \text{ shell count: } y^+_{count} = \sum_{l=1}^{L} \sum_{i=x-l}^{x+l} M(i, y+l), \tag{1}$$

$$\text{Negative } y \text{ shell count: } y^-_{count} = \sum_{l=1}^{L} \sum_{i=x-l}^{x+l} M(i, y-l), \tag{2}$$

$$\text{Positive } x \text{ shell count: } x^+_{count} = \sum_{l=1}^{L} \sum_{j=y-l}^{y+l} M(x+l, j), \tag{3}$$

$$\text{Negative } x \text{ shell count: } x^-_{count} = \sum_{l=1}^{L} \sum_{j=y-l}^{y+l} M(x-l, j). \tag{4}$$

If the reach (search area) of any shell exceeds the domain of the lattice, only the sites

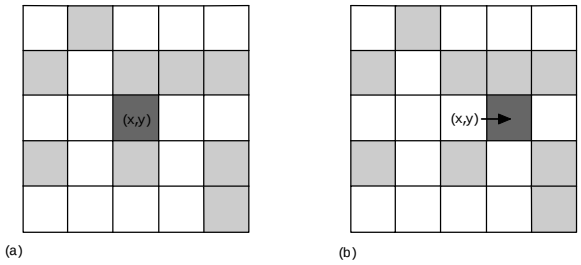

Figure 4: An example of the shell aggregation rule with $L = 2$: The selected agent (dark grey) is located at (x, y), with the light grey sites representing other agents. Here $y^+_{count} = 3, y^-_{count} = 2, x^+_{count} = 4, x^-_{count} = 2$. Hence, in the absence of the random bias component, the agent attempts to move in the positive x direction, and as this site is vacant, the move is successful.

within the domain boundaries are included in the count.

2.2 Random bias component

Given the framework developed in the deterministic component, we now add a random bias mechanism to complete the shell aggregation rule.

For a single application of the deterministic rule, for a chosen agent (x, y), let the total count; $T_{count} = y^+_{count} + y^-_{count} + x^+_{count} + y^-_{count}$.

Now consider the *directional probabilities*;

$$P(y^+) = \frac{y^+_{count}}{T_{count}}, \qquad P(y^-) = \frac{y^-_{count}}{T_{count}}, \qquad P(x^+) = \frac{x^+_{count}}{T_{count}}, \qquad P(x^-) = \frac{x^-_{count}}{T_{count}}.$$

The probabilities sum to 1, and a directional probability will be higher if the respective directional count was larger. Let $S_1 = P(y^+), S_2 = P(y^+) + P(x^+), S_3 = P(y^+) + P(x^+) + P(y^-)$. We can concatenate these into a probability interval between 0 and 1 (represented visually below).

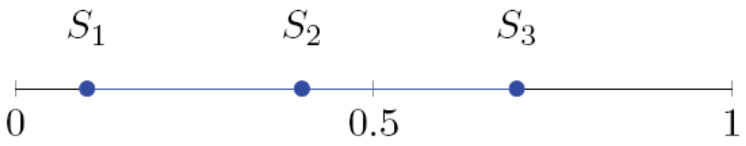

Clearly the widths of these subintervals are equal to the probabilities; $1 - S_3 = P(x^+)$, $S_3 - S_2 = P(y^-)$, $S_2 - S_1 = P(x^+)$ and $S_1 - 0 = P(y^+)$. Consider generating a random number *rand* between 0 and 1. The biased random shell aggregation rule dictates that the agent attempts to;

$$\begin{aligned} \text{Move } y^+ \text{ if } 0 \leq rand \leq S_1 \\ \text{Move } x^+ \text{ if } S_1 < rand \leq S_2 \\ \text{Move } y^- \text{ if } S_2 < rand \leq S_3 \\ \text{Move } x^- \text{ if } S_3 < rand \leq 1 \end{aligned}$$

There is bias for movement to those directions with higher counts, but a level of randomness certainly remains.

3 Results

We now present simulations of the planar aggregation rule. We begin by illustrating our results with images of typical realisations, and then determine a measure of how 'aggregated' a system of agents is. Finally, we investigate the relationship of parameters density, ρ, and search radius, L, on the average area and number of aggregates formed.

A domain of size $X = Y = 100$ is populated randomly with $N = 1000$ agents, corresponding to a density of $\rho = 0.05$. The low density is chosen for ease of viewing cellular behaviour. The aggregation rule is then applied for a prescribed value of L for 1000 time steps. Snapshots are taken at intervals throughout the simulation to show the morphogenesis of the system. The effect of changing L on spatial pattern formation is demonstrated in Figures 5 & 6, with values of $L = 10$ and $L = 30$ respectively. The initial states of the systems have clear areas of concentrated density, and in Figure 5 we see the agents grouping in these areas to form aggregates. In Figure 6, the high value of L causes the agents to all gravitate towards the centre to form one large aggregate.

It quickly became clear that varying search radius, L, and density, ρ, affects the spatial patterns resulting from the application of the shell rule. Whilst the effect of density is more subtle, in Figure 7 we see that increasing L decreases the number of aggregates, and thus increases the size of the aggregates. The effect of both parameters is explored in more detail in Section 3.1. Experimentally, hepatocytes aggregates do not form one large aggregate. While there is much variation in the size of aggregates seen experimentally, those produced by the aggregation rule with $L = 20$ are as large as we have observed. Values of L between 2 and 20 produce spatial patterns most realistic to our application and thus we restrict our attention in analysis of the model to values within this range.

We now discuss how the time to achieve steady-state was determined. For a single cell, an attempted move is aborted if the site it wants to move to according to the rule is occupied. A high count of aborted moves indicates the cells have reached some quasi steady state.
Let $A(t)$ represent the count of aborted moves of the collection of N cells at time t. To

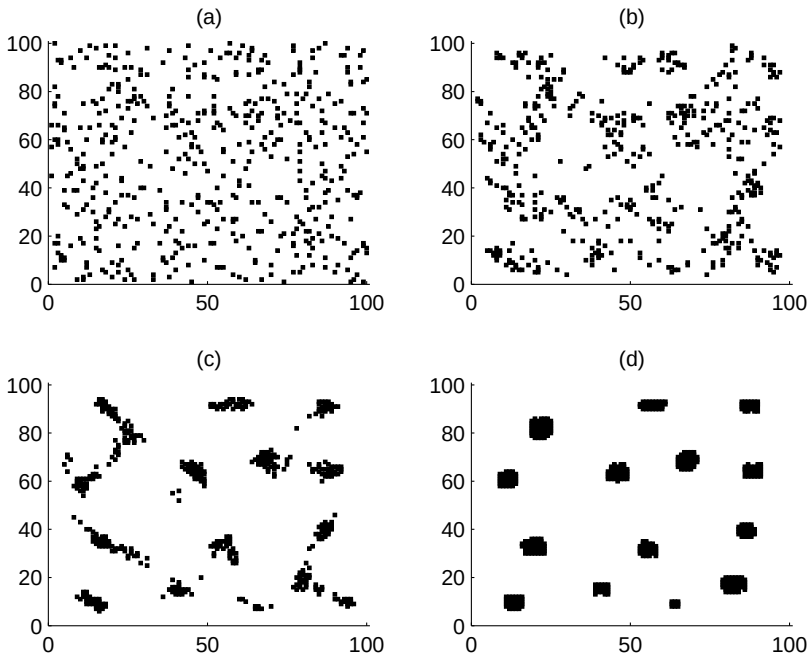

Figure 5: Typical realisation applying the shell aggregation rule on a randomly generated cellular system, with search radius L=10, density fixed at $\rho = 0.05$. Snapshots taken at time steps of interest. (a) t=0 (Initial State), (b) t=12, (c) t=30, (d) t=1000 (Steady State)

investigate the relationship between $A(t)$ and t, we collect data from simulations. Fixing density at ρ=0.1, we generate a random initial system of N agents. For this system, the shell aggregation rule is applied to the population of agents for 300 f time steps. $A(t)$ is recorded at each time step. This process is repeated for 200 realisations and the results are averaged. We present an average aborted count curves for different values of L, (Figure 8(a)), as well as curves representing the standard deviation between samples (Figure 8(b)).

For the deterministic component we expect $\lim_{t\to\infty} A(t) = N$, therefore, we expect that eventually a steady state is reached where all moves aborted. Indeed, we hope that there exists some t_{final} where for all $t \geq t_{final}, A(t) = N$.

However, when the random bias component is incorporated into the aggregation rule, we find that $A(t)$ asymptotes at values slightly below N (see Figure 8(a)). This is reflected in the standard deviation graph, as the curves never reach zero. This behaviour is not unexpected, as while the majority of cells are located in aggregates and are unable to move, there will always be a small number of cells that are either isolated or on the boundary of

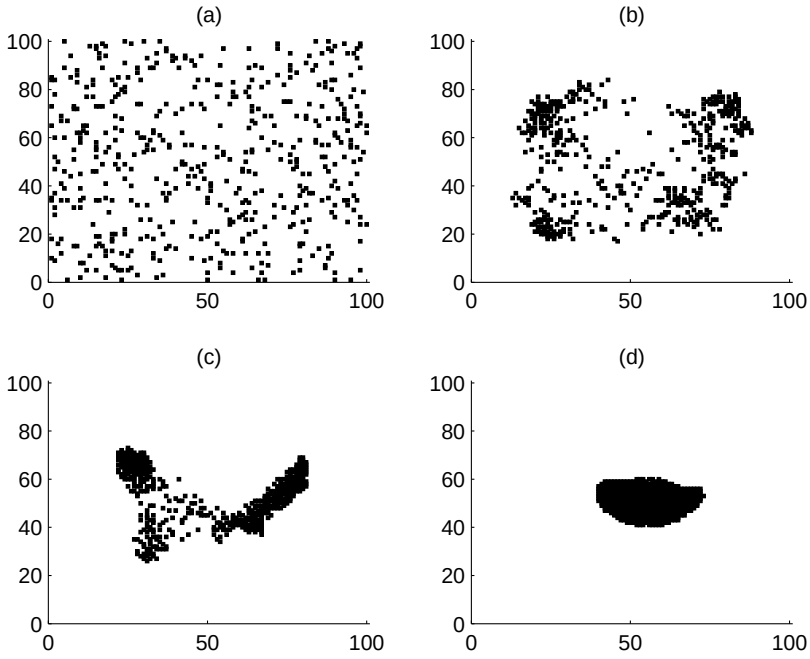

Figure 6: Typical realisation applying the shell aggregation rule on a randomly generated cellular system, with search radius L=30, density fixed at $\rho = 0.05$. Snapshots taken at time steps of interest. (a) t=0 (Initial State), (b) t=40, (c) t=100, (d) t=1000 (Final State)

aggregates. This minority will experience random motion due to the stochastic component of our aggregation rule.

A dominant trend that emerges from the averages graph in Figure 8(a) is that $A(t)$ asymptotes faster with lower values of L, indicating that quasi steady states are achieved faster. This is supported by the peaks in the standard deviation curves (Figure 8(b)), which are higher, wider and take longer to peak for higher values of L. We conclude that by $t = 250$ all systems for $\rho = 0.1$ have achieved a quasi steady state. Thus in future analysis, we simulate up to $t = 1000$ to be confident of full aggregation.

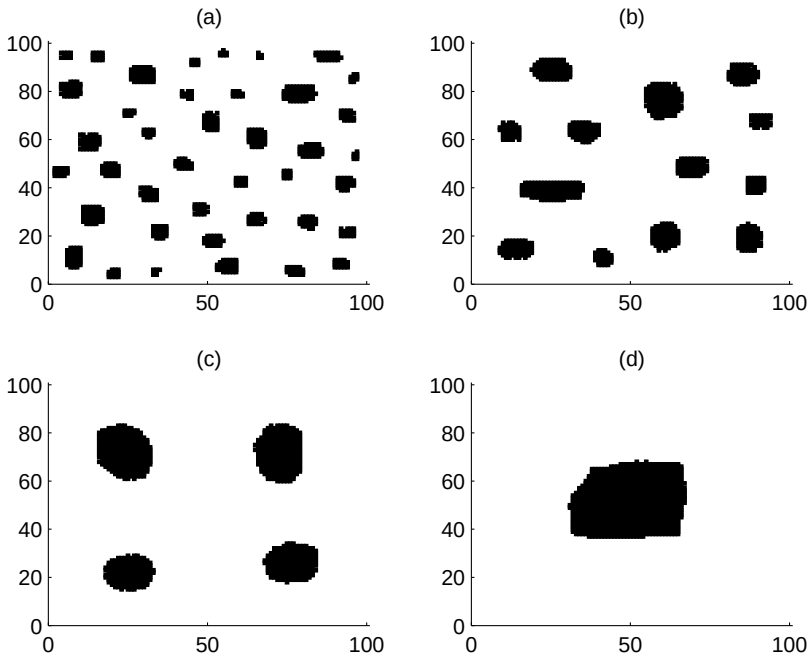

Figure 7: Comparison of (typical realisations) aggregate patterns when varying search radius L, with density fixed at $\rho = 0.1$ (Rule applied to randomly generated initial systems for 1000 time steps). (a) $L = 5$, (b) $L = 10$, (c) $L = 20$, (d) $L = 30$

Postal Address: 111 Barry Street
c/- The University of Melbourne
Victoria 3010 Australia

Email: enquiries@amsi.org.au
Phone: +61 3 8344 1777
Fax: +61 3 9349 4106
Web: www.amsi.org.au

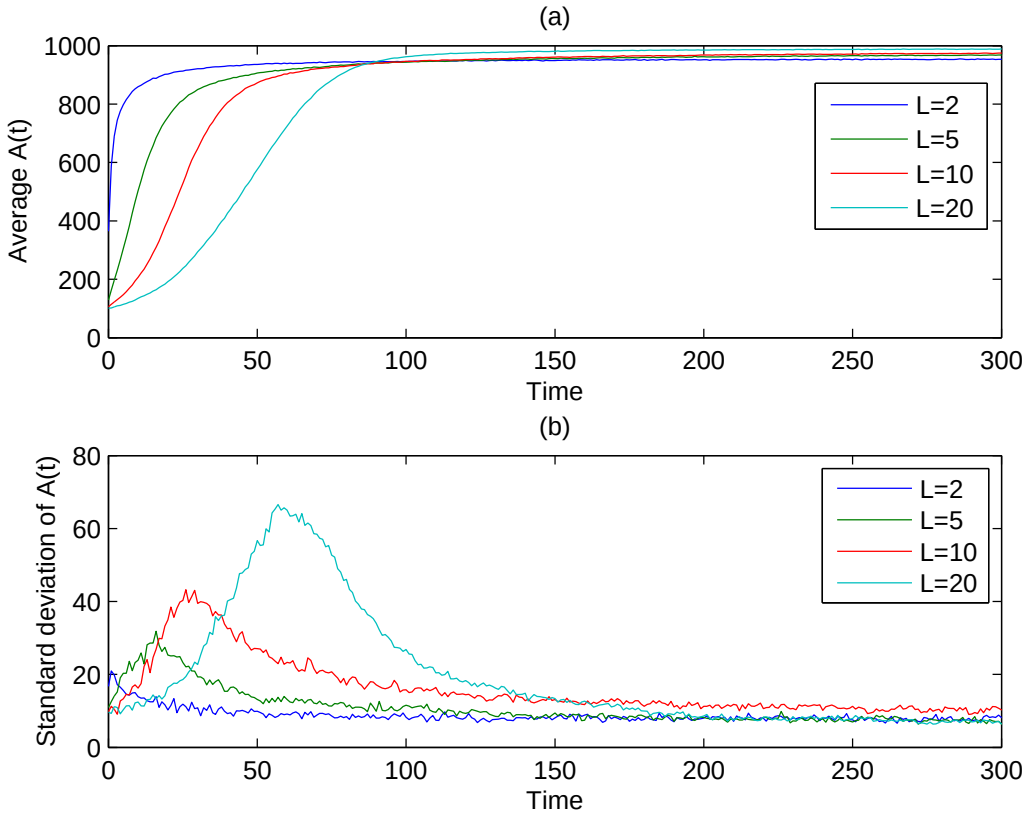

Figure 8: Comparison of average and standard deviation of aborted move count with random bias shell rule. $X = Y = 100$, sample size 200, (ie 200 randomly generated initial systems), varying search radius L, density fixed at $\rho = 0.1$

Postal Address: 111 Barry Street
c/- The University of Melbourne
Victoria 3010 Australia

Email: enquiries@amsi.org.au
Phone: +61 3 8344 1777
Fax: +61 3 9349 4106
Web: www.amsi.org.au

3.1 Aggregate Number and Average Area

Satisfied that the randomly biased shell aggregation rule was producing spatial aggregate patterns that accurately represented the biological process, and with a time of complete aggregation quantified, we now move to quantify the size and number of aggregates produced. As expected, these factors vary with density ρ and search radius L. We seek to investigate this relationship quantitatively using image analysis and statistics.

Once a single simulation i had been completed, and an aggregate pattern realised, image analysis was used to determine number of aggregates A_i and the size of each aggregate. The size of the aggregates was averaged to produce an average size S_i for simulation i.

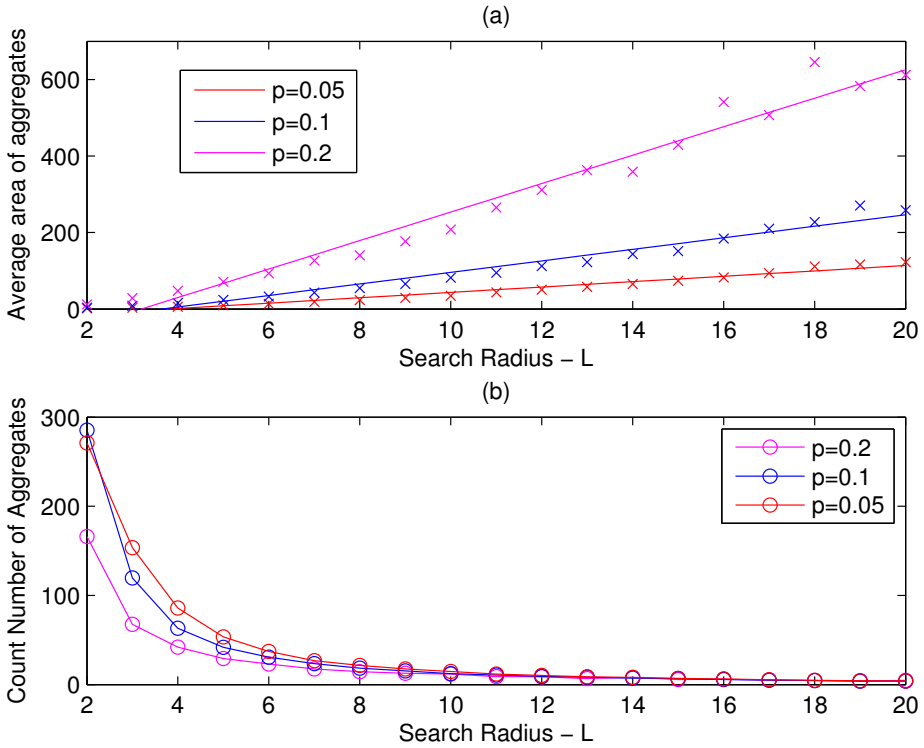

Figure 9: Relationship between length of search radius, L, and resultant (realised) aggregate patterns; (a) Mean average area of aggregates vs length for ρ=0.2, ρ=0.1, ρ=0.05. Averaged over 8 simulations per integer $2 \leq L \leq 30$. Correlation Coefficients r: ρ=0.05, r=0.982, ρ=0.1, r=0.981, ρ=0.2, r=0.983. (b) Average aggregate size vs length for ρ=0.2, ρ=0.1, ρ=0.05. Averaged over 8 simulations per integer $2 \leq L \leq 20$.

We sought to investigate the impact of both search length L and density ρ on values of

A_i and S_i. The random component of the aggregation rule caused considerable variability in the values of A_i and S_i between realisations, even for fixed ρ and L, and due to this the values needed to be averaged.

To do this, values of L, and ρ are fixed, and beginning from a random initial condition, the aggregation rule applied until $t = 1000$. The process is repeated with the same L and ρ, for a specified number (in this case 8) of random initial conditions and A_i and S_i are recorded for each. These values are then averaged to produce mean values of aggregate size and average area of aggregates. This entire process is repeated for increasing values of L (see Figure 9) and ρ (see Figure 10).

The simulation data obtained between search radius, L, on average area of aggregates $\bar{A}$ was found to have a linear relationship. By performing linear regression on the data in Figure (a), it is clear to see that higher densities give larger average aggregate size and larger slopes.

In Figure 9(b), we see that the count number of aggregates, $\bar{S}$, decays quickly as search radius L increases. The difference in $\bar{S}$, for different agent densities is only pronounced for small values of L. We see that higher values of ρ contribute to a smaller number of aggregates for $2 \leq L \leq 10$. Although for $L = 2$, the value of $\bar{S}$ is larger for $\rho = 0.1$ than $\rho = 0.05$, perhaps indicating that larger sample sizes were needed for more consistency.

The data obtained between density of agents, ρ, on $\bar{A}$ and $\bar{S}$ was found to have a linear relationship. The data and respective curve fit are displayed graphically for $L = 5, L = 10, L = 20$ in Figure 10.

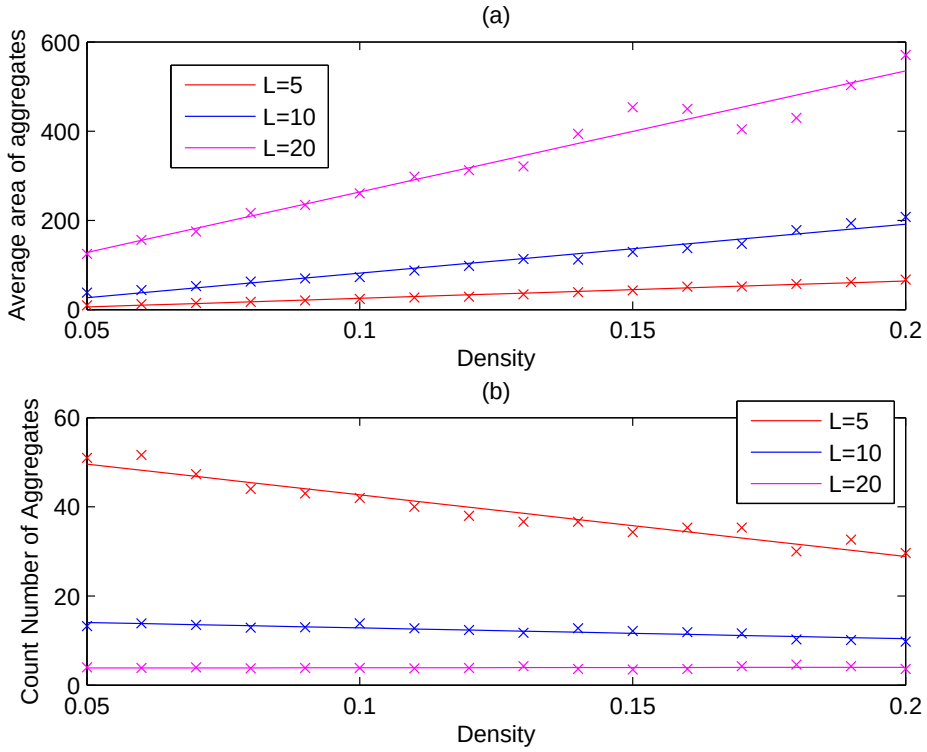

Figure 10: Relationship between density of agents, ρ, on resultant (realised) aggregate patterns. Data and linear regression fits are represented. Data displayed was averaged over 8 simulations per 0.01 increment $0.05 \leq \rho \leq 0.2$. Correlation coefficients r, $L = 5$, $r = 0.993$, $L = 10$, $r = 0.985$, $L = 20$, $r = 0.976$. (a) Mean average area of aggregates vs length for L=2, L=5 and L=10. (b) Average aggregate size vs length for L=2, L=5 and L=10. Correlation coefficients r, $L = 5$, $r = 0.967$, $L = 10$, $r = 0.899$, $L = 20$, $r = 0.164$.

We see in Figure 10(a) that the initial ($\rho = 0.05$) value of $\bar{A}$ increases with L. The slope of the linear fits is also found to increase with L.

In Figure 10(b), we see that the initial ($\rho = 0.05$) value of $\bar{A}$ decreases with increases in L. The slope of the linear fits also appears to decrease with increases in L, confirmed with high correlation in the cases of $L = 5$ and $L = 10$. However, in the case of $L = 20$ a linear fit is found not to be appropriate, with a correlation coefficient of only $r = 0.1640$. Inspection of the data showed that $\bar{S}$ for each ρ was strongly centred about the value 4, with little to no variation initially, and a trend of increasing variation for larger values of ρ. Since 4 is a small number, a variation of 1 is significant, and so while the data is nearly flat here the minimum variation of $\pm 25\%$ causes the poor correlation coefficient.

4 Stacking Rule

While more conventional mono-layer culturing techniques, producing two-dimensional aggregate patterns as modelled above, have been used in the past in generating tissue *in vitro*, recently there has been an emergence of three-dimensional culture techniques. In such environments, hepatocyte cells ultimately form free-floating spheroids. The morphogenesis from randomly dispersed cells on the surface of 2D dish to a fully formed 3D spheroid floating in solution occurs via a number of stages. Initially the cells form planar aggregates (Figure 11 (A)), then the cells stack to form a circular pyramid, and finally cells are able to detach from the surface, forming a spheroid which eventually becomes entirely free-floating (Figure 11 (C) & (D)). Hepatocyte spheroids have been found to have enhanced functionality and viability compared with planar aggregates formed in two-dimensional environments (Thomas et al. (2005)). *In vivo* hepatocytes are found to organise into a three-dimensional structure. Thus it is thought that the two-dimensional environments fail to accurately mimic the natural microenvironment and may impede normal regulatory processes, and that three-dimensional culturing is more suitable for the growth of the structures of hepatocytes found organically (Riccalton-Banks et al. (2003)). For these reasons, we seek to extend the planar model to replicate the early stages of spheroid formation.

4.1 Implementation

We now consider a modification of our aggregation rule which allows cell-stacking. Whereas previously, if the shell rule dictated that an agent sought to move in a direction which was occupied by another agent, the move was aborted, now the motile agent is given an opportunity to stack on top of the occupying agent. This is possible subject to certain constraints, which are increasingly restrictive with respect to the height of the stacks. If the new site is (x, y), then if $M(x, y) = 1$, the chosen agent stacks on the site (*i.e* $M(x, y) = 2$) only if all sites within a 3 site radius (*i.e* 3 squares of lattice sites) are occupied. Similarly, if $M(x, y) = 2$, then $M(x, y)$ can only become 3 only if all sites within a 4 site radius are

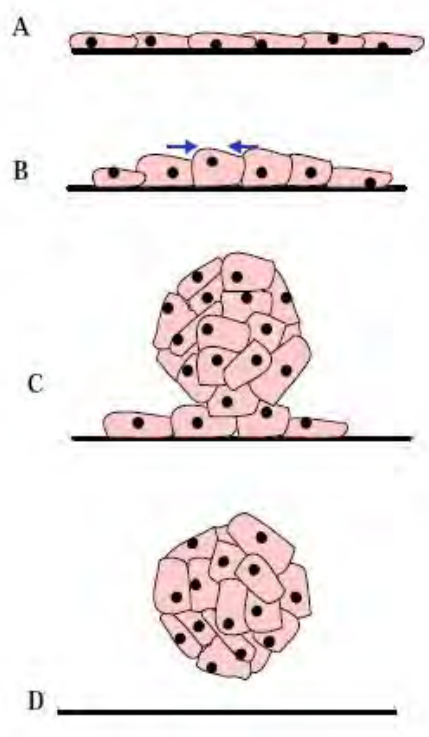

Figure 11: Morphology of spheroid aggregation (from Riccalton-Banks (2002)); (A) Cell clusters form on the surface of the substrate. (B) Clusters begin to contract (arrows indicate direction of contraction). (C) Cell contact with the surface decreases at the centre of the aggregate and a three-dimensional structure is formed. (D) The spheroid detaches from the surface.

occupied. The process continues for all values of $M(x, y)$. This gives a realistic limitation on how high cells can stack, and limits this height respective to the area of the 2D aggregate formed in the first stage of the spheroid formation.

Given this implementation, if $M(x, y) = n > 1$, this represents n agents stacked on top of each other vertically. Thus now when we search for agents to be made motile with aggregation rules, we seek (x, y) such that $M(x, y) \neq 0$. If this is the case, we are only considering that the highest agent on a stack is able to move. So, for example, if $M(x_{current}, y_{current}) = 2$ and $M(x_{new}, y_{new}) = 3$, it is possible given the right conditions that the top cell in the current site could move atop the highest agent on this stack (*i.e* height 3). In this case, we would be left with $M(x_{current}, y_{current}) = 1$ and $M(x_{new}, y_{new}) = 4$. Thus, unlike when stacking is not allowed, where at each time step constant N agents are selected to made motile, now N

is decreased when stacking has occurred. As the agents stack, and N decreases, we are in a sense losing 2D area when looking down on the experimental and simulated images of the cells. Thus we will now refer to the number of agents available for selection as the *planar area*, a time dependent variable $N(t)$. As more agents stack on one another, over time, the number of agents selected for potential motility, $N(t)$, analogous to the planar area, will decrease. As a result, in the aborted moves vs. time plot for the second stage of spheroid formation, we expect to see the count number of aborted moves decreasing over time. Thus, for a measure of steady state, we seek only that the graph asymptotes at some time. In Figures 12 & 13, (a) to (d) show typical realisations of the stacking rule applied to a randomly populated system of agents with density ρ=0.1, and (e) shows the Aborted Moves count $A(t)$, coupled with the Area of cells, $N(t)$. We see in (e) that $N(t)$ increases to a peak, around time $t = 400$. This behaviour before the peak is similar to that observed in the the shell aggregation aborted moves plots, and although the time to peak is not identical, it is close. $N(t)$ stays constant at $N(t) = 1000$, indicating that no stacking is occurring. Both these trends indicate that planar aggregation has been achieved. Thereafter, N(t) decreases with time to an asymptote, in relative synchronisation with the A(t) curve. We see a slightly higher peak in Figure 12 than that of Figure 11, with much higher asymptote in both planar area and aborted moves count. This is reflected by the typical realisations, where we see lower stacking heights in Figure 12 (d) than that of Figure 13 (d). This is expected because for $L = 10$, the stacking process is restricted due to the small size of planar aggregates produced, versus that of $L = 30$ where the large central planar aggregate allows for a large amount of stacking.

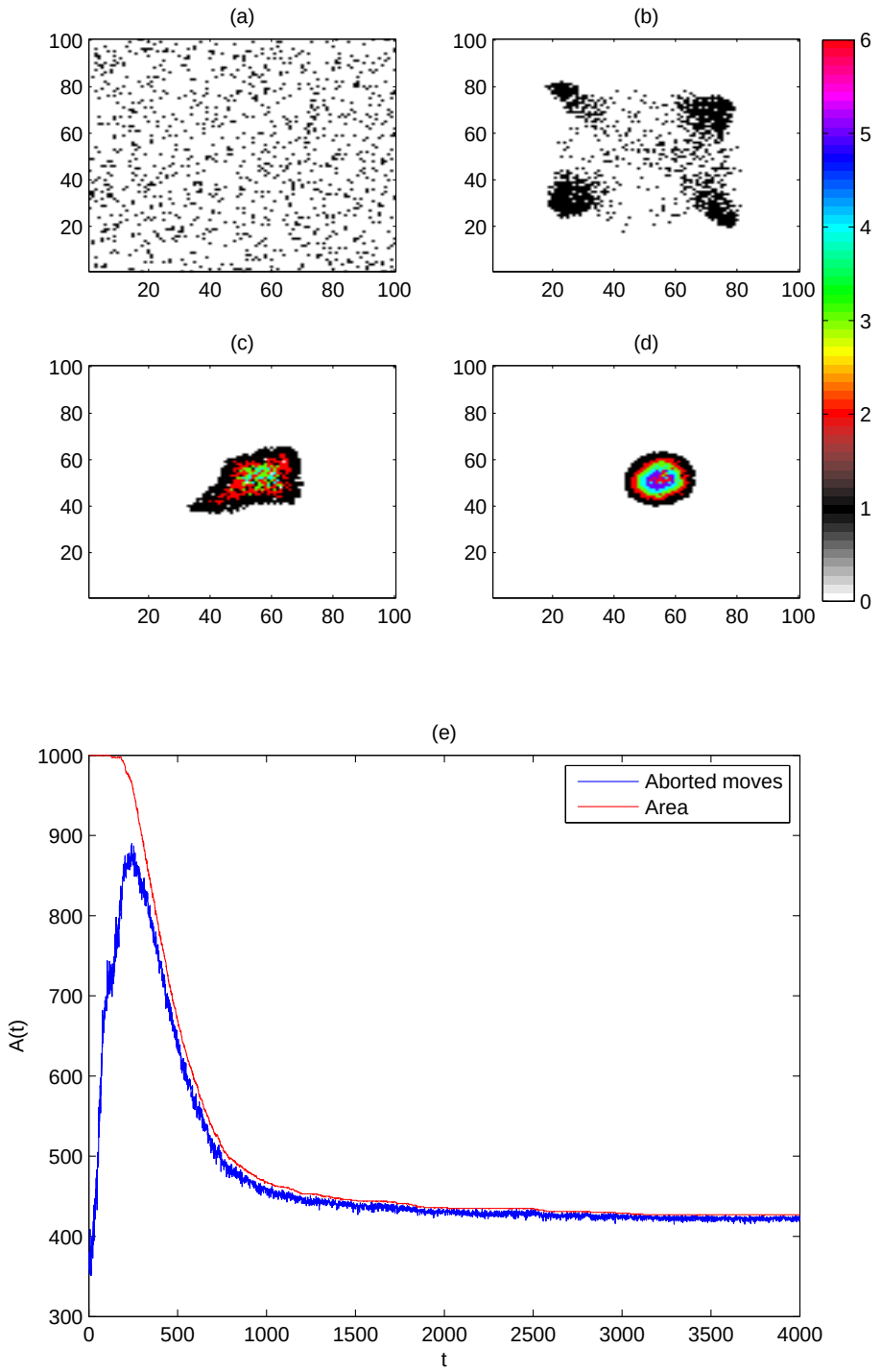

Figure 12: (a)-(d); Snapshots of morphology hepatocyte agents using stacking rule with parameters L=30, $\rho = 0.1$, $X = Y = 100$. (a)$t = 0$, (b) $t = 100$, (c) $t = 500$, (d) $t = 6000$. (e) Aborted moves $A(t)$ and planar area $N(t)$ vs time.

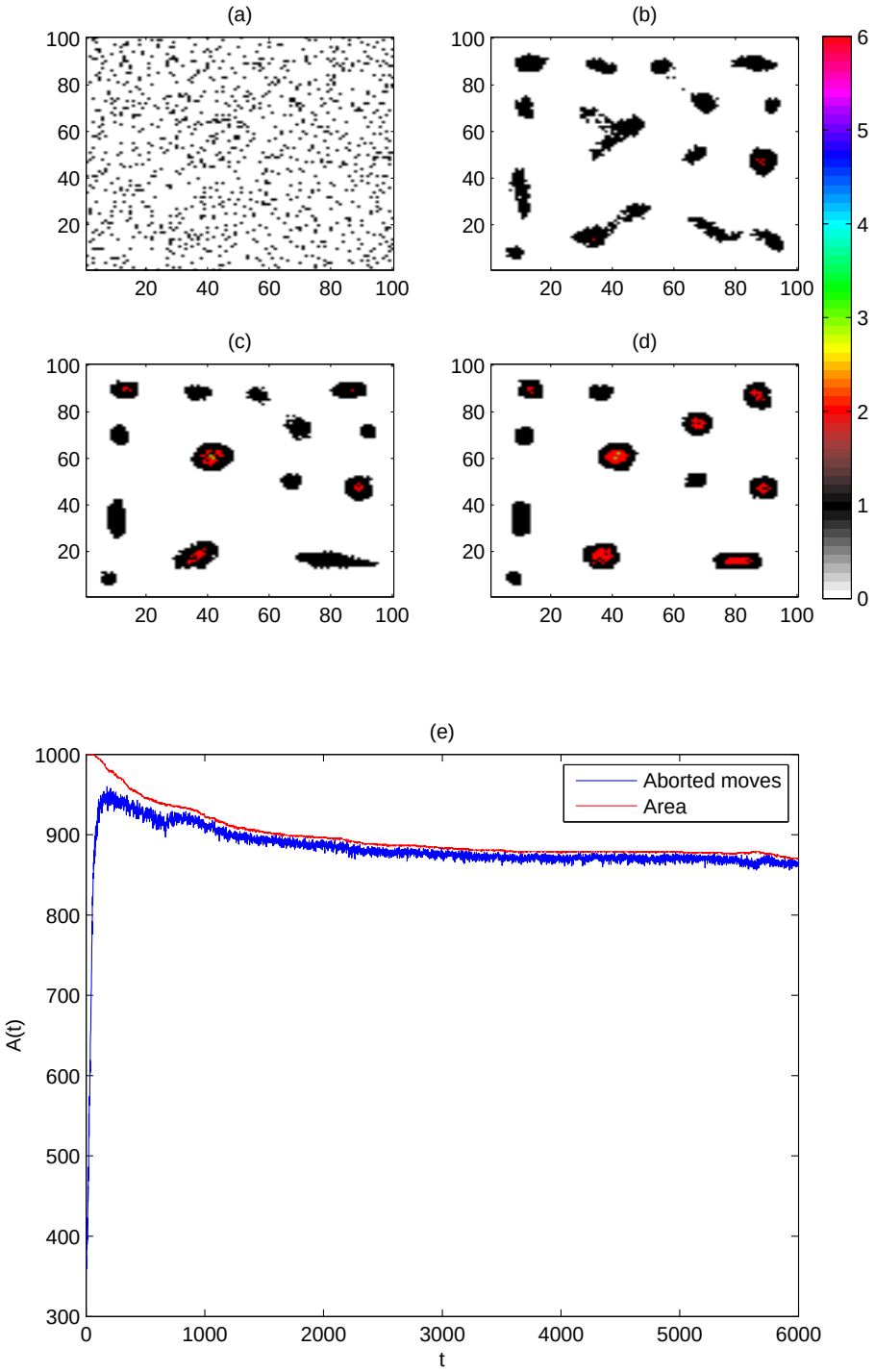

Figure 13: (a)-(d); Snapshots of morphology hepatocyte agents using stacking rule with parameters L=10, $\rho = 0.1$, $X = Y = 100$. (a) $t = 0$, (b) $t = 100$, (c) $t = 500$, (d) $t = 6000$. (e) Aborted moves $A(t)$ and planar area $N(t)$ vs time.

5 A First Step in Calibration - Comparison With Experimental Images

In order to get our planar aggregation and stacking models to best replicate the biological phenomena of hepatocyte aggregation, we need various data to inform how we calibrate the parameters in these models. The following spatial analysis of experimental images is a first step in collecting such data. In reality, more data and possibly more inferences would be needed to accurately inform the calibration. Thus, the methods presented are intended to provide a framework and suggested methodology for obtaining relevant data for extensions on the research in this report. Experimental images of hepatocyte cells co-cultured with stellate cells (other liver cells), provided by The University of Nottingham (RJ. Thomas et al. (2006)) were considered for spatial analysis. The images are taken from a larger domain, with cells moving in and out of the frame. Thus we make the assumption that the net number of cells moving out of the frame is equal to those coming in. Given that our models were based around the movements of a single species of hepatocyte cells, the two-species interactions leading to the aggregation in the experimental images are not represented. As such, whilst the general structure of the aggregated system of cells are similar, we also observe differences between the experimental images and simulated realisations of our model. However, given that hepatocytes are the predominant type of liver cell, the first step in modelling hepatocyte aggregation in the presence of stellate cells was to model and analyse results in absence of stellate cells. A natural extension of this report would be to incorporate stellate cells, and their contribution to the aggregation process. We make use of these images by ignoring the presence of stellate cells.

Firstly, by considering a single image of an aggregated system of hepatocytes *in vitro*, we seek to find an average aggregate size for this image. Figure 14 shows processed images of an experimental aggregate pattern, separating the individual cells from the aggregates. From these images we found that the average aggregate in this experiment consists of approximately 21.41 cells, implying an average aggregate radius of 2.61 cell diameters (assuming circular aggregates). Note that loss of area is not factored into these findings. Using our previous analysis of the planar aggregation model, a value of L could be selected to best match the average size of the aggregates. However, the pronounced variation in aggregate size in the experimental images is not reflected in the model.

In order to calibrate our stacking rule, we seek to quantify a realistic amount of agent-stacking. This can be done by comparing the planar area of the initial and final states of experimental images. Using image processing and analysis on such images, we can find the amount of planar area lost in the aggregation process. This difference in area accounts for how many cells have undergone stacking and thus are 'lost' to the 2D image. Figure 15 shows original and processed images of initial and final states of hepatocyte aggregation in co-culture with stellate cells. We found an initial density of 253.65 cells and a 'loss' of 89.29 cells between images, indicating that approximately 35% of the cells have stacked upon other

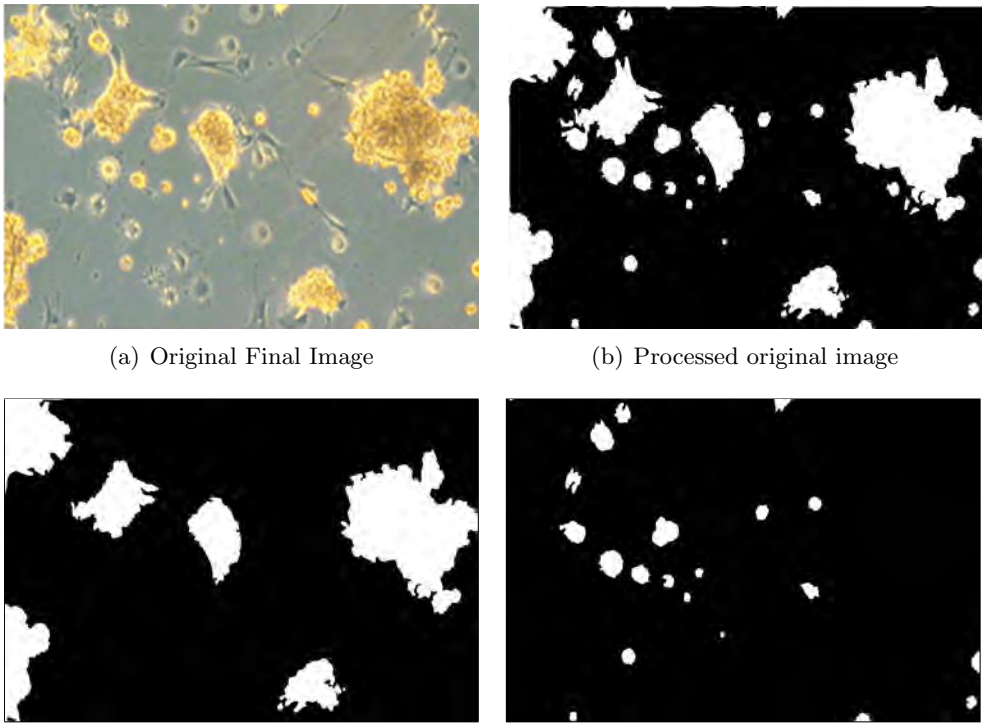

(a) Original Final Image (b) Processed original image

(c) Aggregates extracted (d) Single cells extracted

Figure 14: Image processing is used on an experimental image to isolate individual hepatocyte cells from aggregates in order to estimate their respective area. (a) shows the original image of the final state of the experiment, and (b) is the black and white image produced by image processing. The aggregates and individual cells are then separated into separate images in order to estimate their average area; (c) and (d) respectively.

cells.

It is inherently difficult to cross-compare images between different research groups due to vastly different culturing techniques used. As a result, it is difficult to collect data on a large number of controlled samples. Hence it would be desirable to develop inferential methods on one existing suite of data, or have a much larger suite of data collected experimentally.

6 Discussion

By modelling the aggregation process of single species of cells, with motility based on a combination of cell-cell attraction and random movement, we were able to replicate a wide variety of cell aggregate patterns. We were able to quantify the effect of varying search radius

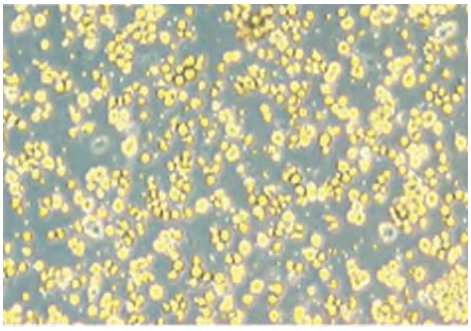

(a) Initial Image

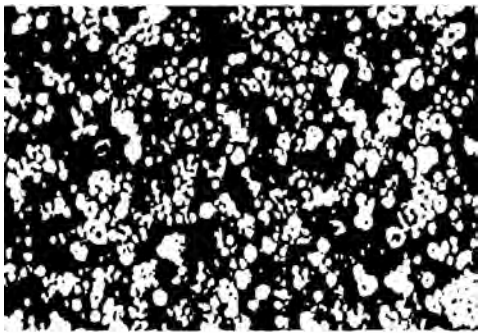

(b) Black and White Image Produced Using Image Processing

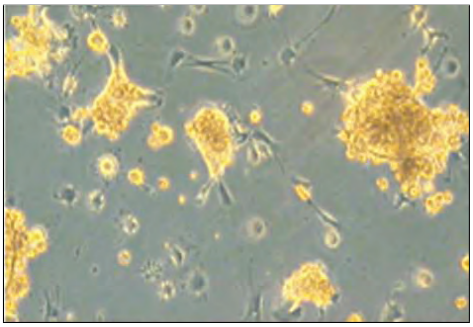

(c) Final Image

(d) Black and White Image Produced Using Image Processing

Figure 15: Using image processing, we calculate the total area of hepatocytes in two experimental images in order to estimate the number of cells stacking on one another. (a) and (b) represent the initial state of the cells before and after image processing, and (c) and (d) represent that of the final state.

and density on the spatial structure of the planar aggregate patterns. The mean average area of aggregates was found to increase linearly with both search radius and density. The count number of aggregates was found to decrease with increases in density and search radius, linearly in the case of the former. We then introduced the first step in a 3D spheroid model; stacking of cells to form a circular pyramid structure. Finally, we developed a proof of concept method for calibration of the models.

Unsurprisingly, the single species model does not match the two species experimental images of aggregation exactly. However, the basic structural elements of the images can be replicated, in particular the potential for the model to be calibrated to produce aggregate patterns of a similar average size to those observed experimentally. This gives us confidence to discuss certain results produced by the model in relation to the underlying biology.

The simulation results make clear the intuitive finding that longer ranges of interactions between cells result in aggregates large in size and few in numbers. This suggests that hepatocyte aggregation is predominantly the result of the cells sensing their immediate environment, as opposed to long range chemical interactions. It is possible that certain environmental factors and culturing techniques change the nature of cell-cell interactions between hepatocytes, effectively changing the search radius. This would explain the variety, particularly size and number, in the aggregate patterns found experimentally between research groups.

While hepatocytes predominate, other cell populations are often integrated in culture. One promising technique to enhance viability and functionality of the tissue is, the introduction of stellate cells to the culture. When co-cultured in three dimensions, hepatocytes and stellates rapidly form heterospheroids. This speed is important for viability, and the resultant heterospheroids have been shown to substantially increase in functionality and viability (Abu-Absi (2004)).

With three-dimensional co-culture dominating the field, the ultimate goal for this report was to contribute to the first stages of an accurate agent-based model of three-dimensional spheroid formation of hepatocyte and stellate cells.
Three important extensions that may be considered together or in parallel would be:

- Collecting or locating more experimental data on co-cultured stellate-hepatocyte aggregation using the image processing as outlined above, and/or considering inference on this data in order to inform the calibration of the aggregation models.
- Integrating stellate cells into the current aggregation model(s), and presenting simulations and analysis of a two species model.
- Extending the 3D spheroid model by continuing the spheroid-aggregation process past the circular pyramid stacking structure. Subsequent stages involve individual cells lifting from the surface, and the group of cells forming a sphere which will eventually lift off the surface entirely. This would involve incorporating cell-surface adhesion strength, and the strength of adhesion compared with cell-cell interactions.

Aggregation is an ubiquitous phenomenon, and as such while the models developed in this report do not yet reflect the complex detail of the intended application, they have the potential to be used in other contexts. Examples may include cell-organ projects in developmental biology, or the study of swarming and social aggregation of animals in ecology.

Acknowledgements

The author acknowledges the financial contribution of the Australian Mathematical Sciences Institute (AMSI) in the production of this report.

References

Abu-Absi, S. F., Hansen L. K. & Hu, W. 2004 Three-dimensional co-culture of hepatocytes and stellate cells. *Cytotechnology* **45**: 125-140, 2004.

Bhandari, R. N. B., Riccalton L. A., Lewis, A. L., Fry J. R., Hammond A. H., Tendler S. J. B. & Shakesheff, K. M 2001 Liver Tissue Engineering: A Role for Co-culture Systems in Modifying Hepatocyte Function and Viability. *Tissue Engineering* Volume 7, Number 3, 2001.

Binder, B. J., Landman, K. A. & Simpson, M. J. with Mariani, M. & Newgreen F. D. 2008 Modeling proliferative tissue growth: A general approach and an avian case study. *The physical review* E **78**, 031912

Binder, B. J. & Landman, K. A. 2009 Exclusion processes on a growing domain *Journal of Theoretical Biology* 259 (2009) 541-551

Edelstein-Keshet, L. 2005 Mathematical Models in Biology *Classics In Applied Mathematics* **46** Society for Industrial and Applied Mathematics (SIAM)

Ermentrout, G. B. & Edelstein-Keshet, L. 1993 Cellular Automata Approaches to Biological Modeling *Journal of Theoretical Biology* 160 (1993) 97-133

Green, J. E. F., Waters, S. L., Whitely, J .P., Edelstein-Keshet, L., Shakesheff, K. M. & Bryne H. M. 2010 Non-local models for the formation of hepatocyte-stellate cell aggregates. *Journal of Theoretical Biology* 267 (20010) 106-120

Hackett-Jones, E. J. & Landman, K. A. with Fellner K. 2012 Aggregation patterns from nonlocal interactions: Discrete stochastic and continuum modelling *The physical review* E **85**, 041912

Kabla, A. J. 2012 Collective cell migration: leadership, invasion and segregation *Interface*, Journal of the Royal Society

Riccalton-Banks, L. 2002 Maintenance of Primary Rat Hepatocytes in vitro Using Co-culture Techniques. PhD thesis, University of Nottingham.

Riccalton-Banks, L., Liew, C., Bhandari, R., Fry, J., & Shakesheff, K. M 2003 Long-Term Culture of Functional Liver Tissue: Three-Dimensional Coculture of Primary Hepatocytes and Stellate Cells. *Tissue Engineering* Volume 9, Number 3, 2003.

Simpson, M. J., Baker, R. E. & McCue S. W. 2011 Models of collective cell spreading with variable cell aspect ratio: A motivation for degenerate diffusion models *The physical review* E **83**, 021901

Thomas, R. J., Bhandari, R., Barrett, D. A., Bennet, A. J., Fry, J. R., Powe, D., Thomson, B. J., & Shakesheff, K. M 2005 The effect of Three-Dimensional Co-Culture of Hepatocytes and Hepatic Stellate Cells on Key Hepatocyte Functions in vitro. *Cells Tissues Organs* 2005; 181:67-79.

Thomas, R. J., Bennet, A., Thomson, B., & Shakesheff, K. M 2006 Hepatic stellate cells on poly(dl-lactic acid) surfaces control the formation of 3D hepatocyte co-culture aggregates *in vitro*. *European Cells and Materials* Vol. 11. 2006 (pages 16-26)